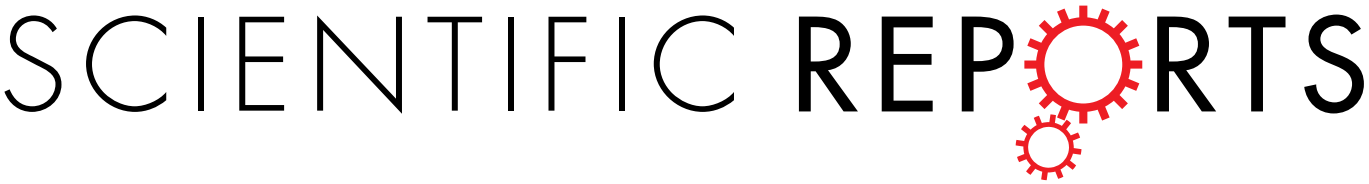

OPEN

Received: 29 September 2016
Accepted: 06 December 2016
Published: 10 January 2017

Characterization of Pairwise Correlations from Multiple Quantum Correlated Beams Generated from Cascaded Four-Wave Mixing Processes

Hailong Wang[1], Leiming Cao[1] & Jietai Jing[1,2]

We theoretically characterize the performance of the pairwise correlations (PCs) from multiple quantum correlated beams based on the cascaded four-wave mixing (FWM) processes. The presence of the PCs with quantum corre- lation in these systems can be verified by calculating the degree of intensity difference squeezing for any pair of all the output fields. The quantum correlation characteristics of all the PCs under different cascaded schemes are also discussed in detail and the repulsion effect between PCs in these cascaded FWM processes is theoretically predicted. Our results open the way for the classification and application of quantum states generated from the cascaded FWM processes.

Quantum correlation shared between multiple quantum correlated beams is important for fundamental quantum mechanics[1] and significant applications in quantum information technologies[2]. The relationship between the quantum correlation shared by the multiple quantum correlated beams and the pairwise correlations (PCs) of the multiple beams remains an open question. For example, ref. 3 discusses the trade-off between A's correlation with B and its correlation with C in a three qubits (A, B and C) system; ref. 4 reviews the properties of the PCs in many-body systems; refs 5, 6 and ref. 7 give the classification of three-qubit correlation and four-qubit correlation respectively which both involve the consideration of PCs. ref. 8 have formalized and extended the operational classification and quantification of multipartite correlated states related to the PCs. Therefore, the characterization of PCs existed in the multiple quantum correlated beams is worth investigating for both the classification and application of quantum states.

Four-wave mixing (FWM) process in a hot rubidium (Rb) vapor[9–24] has several advantages of practical implementations, e.g., no need of cavity due to strong nonlinearity of the system, natural spatial separation of the generated non-classical beams, etc. Our group has experimentally demonstrated the generation of strong quantum correlation between the three bright beams from a cascaded FWM process[25]. Under that experimental condition, there doesn't exist any quantum correlation between any two of the three beams, i. e., no PC with quantum correlation has been shown in our previous work. Therefore, the dependence of the PCs on the system operating condition of the cascaded FWM processes is very interesting and worth studying. In this letter, based on two different cascaded FWM processes, i. e., asymmetrical cascaded scheme and symmetrical cascaded scheme, we theoretically characterize the performance of the PCs of the multiple quantum correlated beams and analyze their dependences on the system intensity gains G_k ($k = 1, 2$). The theoretical predictions can give a rough estimation of the obtained experimental results.

Results

Single FWM scheme. Firstly, we give a simple description of the single FWM scheme. FWM is a nonlinear process in which two pump photons can convert to one signal photon and one idler photon, or vice versa. In the cell_1 of Fig. 1(a), an intense pump beam and a much weaker signal beam are crossed in the center of the Rb vapor

[1]State Key Laboratory of Precision Spectroscopy, School of Physics and Materials Science, East China Normal University, Shanghai 200062, People's Republic of China. [2]Collaborative Innovation Center of Extreme Optics, Shanxi University, Taiyuan, Shanxi 030006, People's Republic of China. Correspondence and requests for materials should be addressed to J.J. (email: jtjing@phy.ecnu.edu.cn)

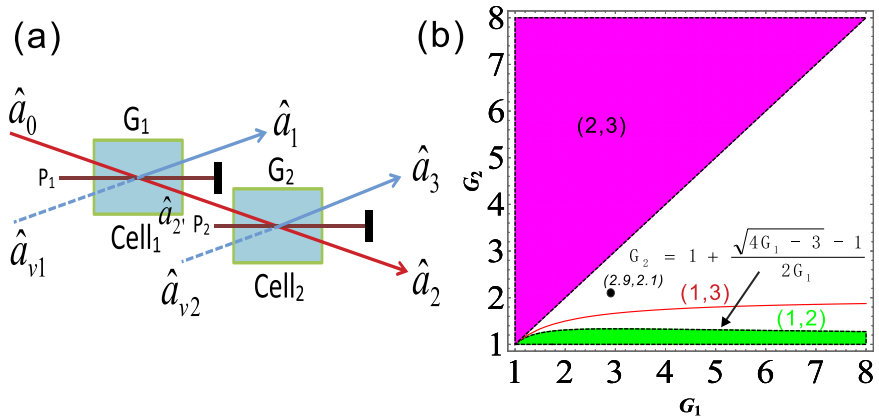

Figure 1. (**a**) Asymmetrical cascaded scheme. $\hat{a}_0$ is coherent input signal, $\hat{a}_{v1}$ and $\hat{a}_{v2}$ are vacuum inputs, G_1 and G_2 are the power gains of cell$_1$ and cell$_2$ respectively. $\hat{a}_{2'}$ is the output signal beam from the first FWM, $\hat{a}_1$, $\hat{a}_2$ and $\hat{a}_3$ are the triple output beams. P_1 and P_2 are the pump beams for the Cell$_1$ and Cell$_2$ respectively. (**b**) The region plot of Eq. (8), Eq. (9) and Eq. (10). The green region (1, 2) is the region of $DS_{12}^2 < 1$, the red line (1, 3) is the region of $DS_{13}^2 = 1$ ($G_2 = 2 - 1/G_1$), the magenta region (2, 3) is the region of $DS_{23}^2 < 1$. The black point (2.9, 2.1) is the experimental gain point. The blank region is the region in which $DS_{12}^2 \geq 1$, $DS_{13}^2 \geq 1$ and $DS_{23}^2 \geq 1$. In all region, $DS_{123}^2 < 1$.

cell with a slight angle. Then the signal beam is amplified as $\hat{a}_{2'}$ and a new beam called idler beam is generated as $\hat{a}_1$ on the other side of the pump beam at the same time. The signal beam and idler beam have different frequencies. The input-output relation of the single FWM scheme shown in Fig. 1(a) is given by

$$\hat{a}_1 = \sqrt{G_1}\hat{a}_{v1} + \sqrt{G_1 - 1}\hat{a}_0^\dagger,\ \hat{a}_{2'} = \sqrt{G_1}\hat{a}_0 + \sqrt{G_1 - 1}\hat{a}_{v1}^\dagger, \tag{1}$$

where G_1 is the power gain of the FWM process. $\hat{a}_{v1}$ is the vacuum input and $\hat{a}_0$ is the coherent input. Following the expressions of the creation and annihilation operators, the optical intensities ($N_i = \hat{a}_i^\dagger \hat{a}_i$ ($i = 1, 2'$)) for the beams $\hat{a}_1$ and $\hat{a}_{2'}$ can be given by

$$\begin{aligned} N_1 &= (G_1 - 1)(N_0 + 1) + \sqrt{G_1(G_1 - 1)}(\hat{a}_0\hat{a}_{v1} + \hat{a}_0^\dagger\hat{a}_{v1}^\dagger), \\ N_{2'} &= G_1 N_0 + \sqrt{G_1(G_1 - 1)}(\hat{a}_0\hat{a}_{v1} + \hat{a}_0^\dagger\hat{a}_{v1}^\dagger), \end{aligned} \tag{2}$$

where $N_0 = \langle \hat{a}_0^\dagger \hat{a}_0 \rangle$. Then the PC for the two beams $\hat{a}_1$ and $\hat{a}_{2'}$ can be quantified by the degree of intensity difference squeezing (DS), i. e., the ratio of the variance of the correlated beams to the variance at the standard quantum limit (SQL)[26]

$$DS_{12'}^1 = \frac{Var(N_1 - N_{2'})_{FWM}}{Var(N_1 - N_{2'})_{SQL}} = \frac{1}{2G_1 - 1}, \tag{3}$$

here $Var(N_1 - N_{2'})_{FWM} = Var(-N_0 + G_1 - 1)_{FWM} \approx N_0$ and $Var(N_1 - N_{2'})_{SQL} = \langle (2G_1 - 1)N_0 + G_1 - 1 \rangle \approx (2G_1 - 1)N_0$. Here the superscript and subscript for the DS_{ij}^k represent the kth ($k = 1, 2, 3$) scheme (we have three schemes throughout the whole discussion, i. e., the single FWM scheme (1), the asymmetrical cascaded scheme (2) and the symmetrical cascaded scheme (3), the ith ($i = 1, 2, 3$) beam and the jth ($j = 2', 2, 3, 4$) beam in the scheme. $Var(A) = \langle A^2 \rangle - \langle A \rangle^2$ denotes the variance of A. $DS_{12'}^1 < 1$ demonstrates the presence of PC with quantum correlation between the two beams from the FWM process. Since G_1 is always larger than 1, the PC with quantum correlation of the two beams can be easily obtained in the experiment. However, the DSs of the single beams $\hat{a}_1$ and $\hat{a}_{2'}$ are given by

$$\begin{aligned} DS_1^1 &= \frac{Var(N_1)_{FWM}}{Var(N_1)_{SQL}} = \frac{G_1(G_1 - 1)N_0 + (G_1 - 1)^2 N_0}{(G_1 - 1)N_0} = 2G_1 - 1, \\ DS_{2'}^1 &= \frac{Var(N_{2'})_{FWM}}{Var(N_{2'})_{SQL}} = \frac{G_1(G_1 - 1)N_0 + G_1^2 N_0}{G_1 N_0} = 2G_1 - 1. \end{aligned} \tag{4}$$

This corresponds to a linear increase in the noise on both the signal and idler beams as gain is increased. Thus the beams $\hat{a}_1$ and $\hat{a}_{2'}$ in the FWM process are both in thermal states.

Asymmetrical cascaded FWM scheme. Secondly, compared to the above mentioned single FWM scheme, here we construct the asymmetrical cascaded scheme in Fig. 1(a). We take the signal beam from the first FWM process (cell$_1$) as the seed for the second FWM process (cell$_2$) in Fig. 1(a)[25]. $\hat{a}_1$, $\hat{a}_2$ and $\hat{a}_3$ are three

newly-generated beams in the output stage of the cascaded processes. In our previous work[25], we have shown the generation of strong quantum correlation between the three bright beams but not the PCs with quantum correlation for any pair of the three beams. Here we will study all the PCs of the triple beams $\hat{a}_1$, $\hat{a}_2$ and $\hat{a}_3$ in Fig. 1(a) and look for the possibilities for the existence of PCs with quantum correlation. The input-output relation of the asymmetrical cascaded scheme in Fig. 1(a) can be written as

$$\begin{aligned}\hat{a}_1 &= \sqrt{G_1}\hat{a}_{\nu 1} + \sqrt{G_1 - 1}\hat{a}_0^\dagger,\\ \hat{a}_2 &= \sqrt{G_1 G_2}\hat{a}_0 + \sqrt{G_2(G_1 - 1)}\hat{a}_{\nu 1}^\dagger + \sqrt{G_2 - 1}\hat{a}_{\nu 2}^\dagger,\\ \hat{a}_3 &= \sqrt{G_2}\hat{a}_{\nu 2} + \sqrt{G_1(G_2 - 1)}\hat{a}_0^\dagger\\ &\quad + \sqrt{(G_1 - 1)(G_2 - 1)}\hat{a}_{\nu 1},\end{aligned} \tag{5}$$

where G_1 and G_2 are the power gains for the cell$_1$ and cell$_2$ respectively. The optical intensities ($N_i = \hat{a}_i^\dagger \hat{a}_i$ ($i = 1, 2$ and 3)) for the individual beams $\hat{a}_1$, $\hat{a}_2$ and $\hat{a}_3$ can be given by

$$\begin{aligned}N_1 &= (G_1 - 1)(N_0 + 1) + \sqrt{G_1(G_1 - 1)}(\hat{a}_0\hat{a}_{\nu 1} + \hat{a}_0^\dagger\hat{a}_{\nu 1}^\dagger),\\ N_2 &= G_1 G_2 N_0 + G_2\sqrt{G_1(G_1 - 1)}(\hat{a}_0\hat{a}_{\nu 1} + \hat{a}_0^\dagger\hat{a}_{\nu 1}^\dagger)\\ &\quad + \sqrt{G_1 G_2(G_2 - 1)}(\hat{a}_0\hat{a}_{\nu 2} + \hat{a}_0^+\hat{a}_{\nu 2}^\dagger),\\ N_3 &= G_1(G_2 - 1)(N_0 + 1)\\ &\quad + (G_2 - 1)\sqrt{G_1(G_1 - 1)}(\hat{a}_0\hat{a}_{\nu 1} + \hat{a}_0^\dagger\hat{a}_{\nu 1}^\dagger)\\ &\quad + \sqrt{G_1 G_2(G_2 - 1)}(\hat{a}_0\hat{a}_{\nu 2} + \hat{a}_0^\dagger\hat{a}_{\nu 2}^\dagger),\end{aligned} \tag{6}$$

where $N_0 = \langle \hat{a}_0^\dagger \hat{a}_0 \rangle$. Here the second-order vacuum terms are omitted. It should be noted that the *DS* of the triple beams ($\hat{a}_1$, $\hat{a}_2$ and $\hat{a}_3$) is given by

$$DS_{123}^2 = \frac{Var(N_2 - N_1 - N_3)_{FWM}}{Var(N_2 - N_1 - N_3)_{SQL}} = \frac{1}{2G_1 G_2 - 1}, \tag{7}$$

where G_1 and G_2 are the power gains for the two FWM processes. Compared with Eq. (3), Eq. (7) means that the cascaded FWM process can enhance the quantum correlation of the system. The symmetrical dependence of the DS_{123}^2 on the gains is shown in Fig. 2(a) and can be enhanced with the increasing of the gains G_1 and G_2. The quantum correlation shared by the triple beams is present if $G_1 G_2 > 1$, i. e., $G_1 > 1$ or $G_2 > 1$.

Next we analyze all the possible PCs using the *DS* criterion. PC between $\hat{a}_1$ and $\hat{a}_2$ can be quantified by

$$DS_{12}^2 = \frac{2G_1^2 G_2^2 - 4G_1^2 G_2 + 2G_1^2 + 3G_1 G_2 - 3G_1 + 1}{G_1 G_2 + G_1 - 1}. \tag{8}$$

Eq. (8) will be reduced to $2G_2 - 1$ and $1/(2G_1 - 1)$ when we set $G_1 = 1$ and $G_2 = 1$ respectively, corresponding to the cases of Eq. (4) and Eq. (3) respectively. These phenomena can be understood as follows. When we set $G_1 = 1$, the PC between the thermal states $\hat{a}_1$ and $\hat{a}_2$ translates into the one between the vacuum state $\hat{a}_1$ and the thermal state $\hat{a}_2$, i. e., $DS_{12}^2 = 2G_2 - 1$. When we set $G_2 = 1$, the PC between the thermal states $\hat{a}_1$ and $\hat{a}_2$ translates into the one between the twin beams from the first FWM process, i. e., $DS_{12}^2 = 1/(2G_1 - 1)$. The region in which $DS_{12}^2 < 1$, i. e., there exists quantum correlation between beams $\hat{a}_1$ and $\hat{a}_2$, is shown in green denoted as (1, 2) in Fig. 1(b). The value of G_2 on the boundary (see the boundary given by $G_2 = 1 + (\sqrt{4G_1 - 3} - 1)/2G_1$ in Fig. 1(b)) of that region reaches its maximal value of 1.33 when $G_1 = 3$ and it decreases when $G_1 > 3$ and will eventually reaches at the value of 1. To clearly see how the DS_{12}^2 depends on the gains G_1 and G_2, the contour plot of it is shown in Fig. 2(b). The larger G_1 and smaller G_2 are preferred for achieving $DS_{12}^2 < 1$. The study of DS_{12}^2 presented above is actually the question of how to preserve the quantum correlation between beams $\hat{a}_1$ and $\hat{a}_2$ under the introduction of a second FWM which brings the deterioration effect to the quantum correlation by the quantum amplification of one of the beams ($\hat{a}_2$). The results shown in Figs 1(b) and 2(b) actually shows the value of G_2 on the boundary below which the quantum correlation can always be preserved as the value of G_1 increases. That is to say, in the low gain regime ($G_1 < 3$), the stronger the quantum correlation between beams $\hat{a}_1$ and $\hat{a}_2$ is, the more robust to the deterioration effect from the quantum amplification of the second FWM it becomes. More interestingly, in the high gain regime ($G_1 > 3$), the stronger the quantum correlation between beams $\hat{a}_1$ and $\hat{a}_2$ is, the more fragile to the deterioration effect from the quantum amplification of the second FWM it becomes.

PC between $\hat{a}_1$ and $\hat{a}_3$ can be quantified by

$$DS_{13}^2 = \frac{2G_1^2 G_2^2 - 8G_1^2 G_2 + 8G_1^2 + 5G_1 G_2 - 8G_1 + 1}{G_1 G_2 - 1}. \tag{9}$$

Eq. (9) is equal to 1 when $G_2 = 2 - 1/G_1$, meaning that the quantum fluctuation of intensity difference of two thermal states can be equal to the one of two coherent states with equal powers. Except that, DS_{13}^2 is always larger than 1, i. e., there is no quantum correlation between beams $\hat{a}_1$ and $\hat{a}_3$. The region in which $DS_{13}^2 = 1$ ($G_2 = 2 - 1/G_1$) is shown as the red line denoted as (1, 3) in Fig. 1(b). The contour plot of DS_{13}^2 is also shown in

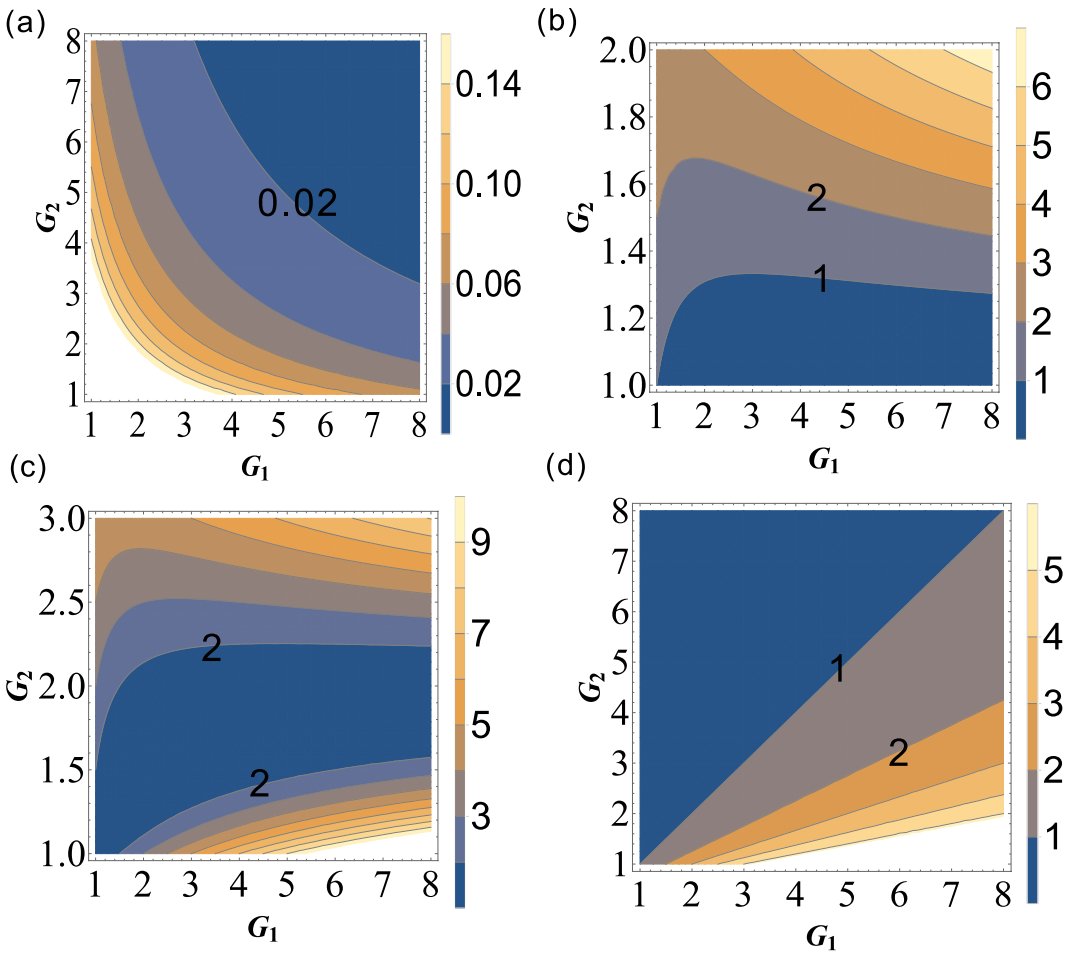

Figure 2. The contour plot of (**a**) DS^2_{123}; (**b**) DS^2_{12}; (**c**) DS^2_{13} and (**d**) DS^2_{23}.

Fig. 2(c) in which the value of all the region is more than or equal to 1 for any G_1, $G_2 > 1$. In this sense, there isn't any quantum correlation between beams $\hat{a}_1$ and $\hat{a}_3$ for any value of G_1 and G_2 since DS^2_{13} is always more than or equal to 1.

PC between $\hat{a}_2$ and $\hat{a}_3$ can be quantified by

$$DS^2_{23} = \frac{2G_1 - 1}{2G_2 - 1}. \tag{10}$$

The simplified results, i. e., $1/(2G_2 - 1)$ and $2G_1 - 1$ for Eq. (10) can be obtained when G_1 and G_2 are set to equal to 1 respectively, corresponding to the cases of Eq. (3) and Eq. (4) respectively. This is because when we set $G_1 = 1$, the PC between the thermal states $\hat{a}_2$ and $\hat{a}_3$ translates into the one between the twin beams from the second FWM process, i. e., $DS^2_{23} = 1/(2G_2 - 1)$. When we set $G_2 = 1$, the PC between the thermal states $\hat{a}_2$ and $\hat{a}_3$ translates into the one between the thermal state $\hat{a}_2$ and the vacuum state $\hat{a}_3$, i. e., $DS^2_{23} = 2G_1 - 1$. The region in which $DS^2_{23} < 1$ ($G_1 < G_2$) is shown in magenta denoted as (2, 3) in Fig. 1(b), meanwhile, the contour plot of DS^2_{23} is also shown in Fig. 2(d) in which the region of $G_1 < G_2$ gives $DS^2_{23} < 1$. Therefore, the PC with quantum correlation between beams $\hat{a}_2$ and $\hat{a}_3$ will be present for any G_1 less than G_2. This is not difficult to figure out if one looks at the functional form of Eq. (10). As we all know, in order to generate strong quantum correlation from FWM process, the shot noise limited seed beam, such as coherent state or vacuum state, is always preferred. From this point of view, the analysis presented above actually answers the question of how to produce quantum correlation with the seeding of a thermal state. Figs 1(b) and 2(d) actually gives the answer that the quantum correlation will be produced as long as the FWM gain for producing the quantum correlation is larger than the FWM gain for the thermal state generation. In such region ($G_1 < G_2$), the existence of quantum correlation between beams $\hat{a}_2$ and $\hat{a}_3$ eliminates the possibility of the one between beams $\hat{a}_2$ and $\hat{a}_1$. In other words, beam $\hat{a}_2$ can't be simultaneously quantum correlated with beams $\hat{a}_1$ and $\hat{a}_3$. In this sense, we could call this phenomena as repulsion effect of quantum correlation between the PCs in this cascaded FWM process. It can be explained as follows. The repulsion effect is actually the result of the competition between the correlation mechanism and decorrelation mechanism. As shown in Fig. 1(a), firstly, for the PC between beams $\hat{a}_1$ and $\hat{a}_2$, obviously, cell$_1$ will provide the correlation between them and cell$_2$ will destroy their quantum correlation by adding extra vacuum noise, thus cell$_1$ and cell$_2$

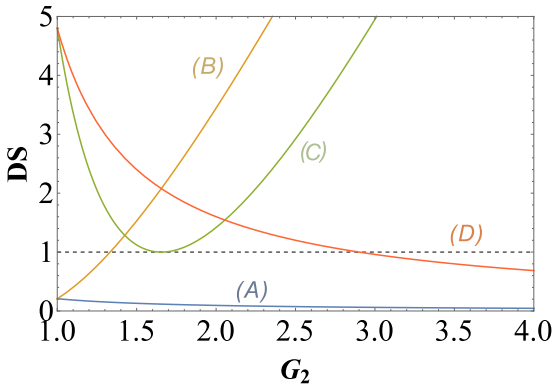

Figure 3. The dependence of (*A*) DS^2_{123}; (*B*) DS^2_{12}; (*C*) DS^2_{13} and (*D*) DS^2_{23} on the gain G_2 when $G_1 = 2.9$ ($cell_1$ gain in the experiment). The black dashed line: SQL.

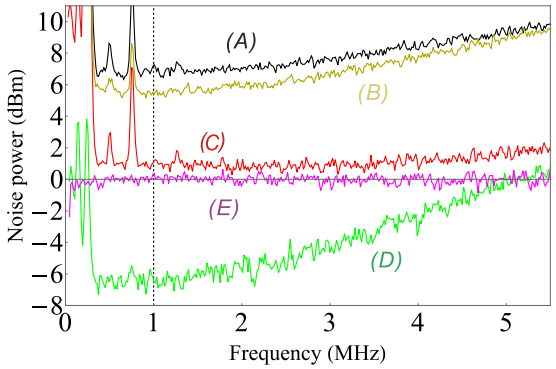

Figure 4. Experimentally measured (*A*) DS^2_{12}; (*B*) DS^2_{13}; (*C*) DS^2_{23}; (*D*) DS^2_{123} and (*E*) the corresponding SQLs of the traces *A* ~ *D* in the asymmetrical cascaded scheme. The vertical dashed line: 1 MHz.

can be viewed as the correlation mechanism provider and decorrelation mechanism provider respectively, thus the larger G_1 and smaller G_2 are preferred for the PC between beams $\hat{a}_1$ and $\hat{a}_2$. Secondly, for the case of the PC between beams $\hat{a}_2$ and $\hat{a}_3$, $cell_1$ will generate a thermal state $\hat{a}_{2'}$ which will destroy their quantum correlation by adding extra vacuum noise into the system while the $cell_2$ will make them quantum correlated through the FWM process. In this case, $cell_1$ and $cell_2$ can be viewed as the decorrelation mechanism provider and correlation mechanism provider respectively, thus the smaller G_1 and larger G_2 are preferred for the PC between beams $\hat{a}_2$ and $\hat{a}_3$. Finally, the complete opposite dependence of the PC between beams $\hat{a}_1$ and $\hat{a}_2$ and the PC between beams $\hat{a}_2$ and $\hat{a}_3$ on the gains leads to the repulsion effect between the PCs of certain pairs. In the blank region of Fig. 1(b), all the PCs with quantum correlation are absent since $DS^2_{12} \geq 1$, $DS^2_{13} \geq 1$ and $DS^2_{23} \geq 1$, however, the quantum correlation between the triple beams is still present.

In order to give a summary of the theoretical predictions of Figs 1(b) and 2. We plot the dependence of (A) DS^2_{123}; (B) DS^2_{12}; (C) DS^2_{13} and (D) DS^2_{23} on the gain G_2 when $G_1 = 2.9$ ($cell_1$ gain in the experiment) in Fig. 3. DS^2_{123} (trace A) can be enhanced with the increasing of G_2 which is consistent with Fig. 2(a), the value of DS^2_{12} (trace B) will be larger than 1 as long as $G_2 > 1.33$ which is consistent with the boundary of DS^2_{12} in Fig. 1(b), DS^2_{13} (trace C) will approach the SQL only $G_2 = 1.66$ which is consistent with $G_2 = 2 - 1/G_1$ in Fig. 1(b), the value of DS^2_{23} (trace D) will be smaller than 1 as long as $G_2 > 2.9$ which is consistent with Figs 1(b) and 2(d).

To verify these theoretical predictions, we apply them to the experimental results. The measured results are shown in Fig. 4, the traces *A*, *B*, *C* and *D* are the measured DSs between $\hat{a}_1$ and $\hat{a}_2$, $\hat{a}_1$ and $\hat{a}_3$, $\hat{a}_2$ and $\hat{a}_3$ and the triple beams respectively, the trace *E* is the corresponding normalized SQLs for traces *A* ~ *D* (See the methods). The experimental results show $10\text{Log}(DS^2_{12}) = 7.0 \pm 0.2$ dB, $10\text{Log}(DS^2_{13}) = 5.5 \pm 0.1$ dB, $10\text{Log}(DS^2_{23}) = 1.0 \pm 0.2$ dB and $10\text{Log}(DS^2_{123}) = -6.7 \pm 0.4$ dB at 1 MHz where the maximal degree of squeezing can be considered as the best choice to reflect the quantum properties of the system because there exist huge classical noise peaks at lower frequencies from the laser, the bandwidth limitation of the photodetector and even the bandwidth limitation of the squeezing generation. As we can see from Fig. 4, the noise power of the three beams increases quickly as the frequency increases. It also increases faster than the one of the two beams. We can understand this results as follows. Although the probe and idler beams in the single FWM scheme are generated almost simultaneously, there are still some time delay between them during their propagation through the cell[27]. This difference limits the squeezing bandwidth to some extent. This time delay induced squeezing bandwidth becomes narrower in the case of asymmetrical cascaded FWM scheme due to two of the three beams experiencing additional time delay in the

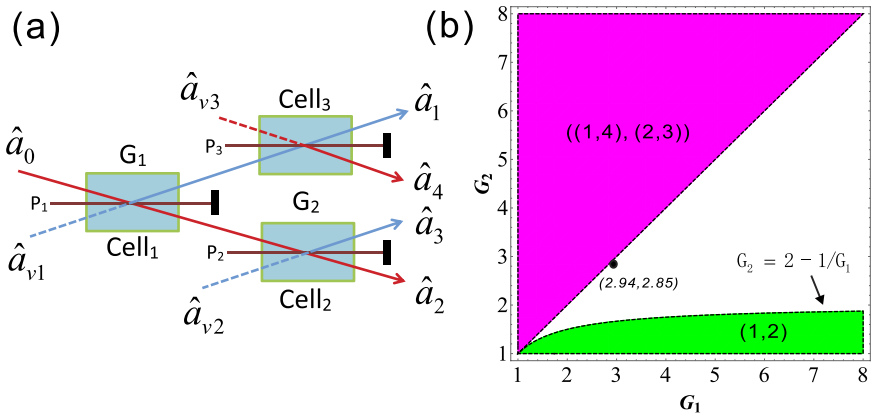

Figure 5. (**a**) Symmetrical cascaded scheme. $\hat{a}_0$ is coherent input signal, $\hat{a}_{v1}$, $\hat{a}_{v2}$ and $\hat{a}_{v3}$ are vacuum inputs, G_1 and G_2 are the power gains of cell$_1$ and cell$_2$ (cell$_3$) respectively. $\hat{a}_1$, $\hat{a}_2$, $\hat{a}_3$ and $\hat{a}_4$ are the output beams. P_1, P_2 and P_3 are the pump beams for the Cell$_1$, Cell$_2$ and Cell$_3$ respectively. (**b**) The region plot of Eq. (14), Eq. (15). The green region (1, 2) is the region of $DS^3_{12} < 1$, the magenta region ((1, 4), (2, 3)) is the region of $DS^3_{14} < 1$ and $DS^3_{23} < 1$. The black point (2.94, 2.85) is the experimental gain point. The blank region is the region of $DS^3_{12} \geq 1$, $DS^3_{13} \geq 1$, $DS^3_{14} \geq 1$, $DS^3_{23} \geq 1$, $DS^3_{24} \geq 1$ and $DS^3_{34} \geq 1$, meaning that there is no PC with quantum correlation for any pair of the quadruple beams. In all region, $DS^3_{1234} < 1$.

second vapor cell. The faster increasing of the noise power of the three beams than the one of the two beams is due to that the number of beams of the three beams related to the time delay is more than the one of the two beams. For the experimental gains $G_1 \approx 2.9$ and $G_2 \approx 2.1$, our theoretical predictions give $10\text{Log}(\text{DS}^2_{12}) = 5.9$ dB, $10\text{Log}(\text{DS}^2_{13}) = 2.2$ dB, $10\text{Log}(\text{DS}^2_{23}) = 1.8$ dB and $10\text{Log}(\text{DS}^2_{123}) = -10.5$ dB in which the positive and negative values represent antisqueezing and squeezing respectively. As we can see, although these theoretical predictions do not perfectly agree with the experimental results at 1 MHz, they still give a rough estimation of the relationship between the obtained experimental noise power traces.

Symmetrical cascaded FWM scheme. Finally, we construct the following symmetrical cascaded scheme as shown in Fig. 5(a). We take the signal beam from the first FWM process (cell$_1$) as the seed for the second FWM process (cell$_2$) and the idler beam as the seed for the third FWM process (cell$_3$) in Fig. 5(a). $\hat{a}_1$, $\hat{a}_2$, $\hat{a}_3$ and $\hat{a}_4$ are the quadruple newly-generated beams in the output stage of the cascaded processes. We will also study all the PCs of the quadruple beams $\hat{a}_1$, $\hat{a}_2$, $\hat{a}_3$ and $\hat{a}_4$ in Fig. 5(a) and look for the possibilities for existence of the PCs with quantum correlation. The input-output relation of the symmetrical cascaded scheme in Fig. 5(a) can be written as

$$\begin{aligned}
\hat{a}_1 &= \sqrt{G_1G_2}\,\hat{a}_{v1} + \sqrt{G_2(G_1-1)}\,\hat{a}_0^\dagger + \sqrt{G_2-1}\,\hat{a}_{v3}^\dagger,\\
\hat{a}_2 &= \sqrt{G_1G_2}\,\hat{a}_0 + \sqrt{G_2(G_1-1)}\,\hat{a}_{v1}^\dagger + \sqrt{G_2-1}\,\hat{a}_{v2}^\dagger,\\
\hat{a}_3 &= \sqrt{G_2}\,\hat{a}_{v2} + \sqrt{G_1(G_2-1)}\,\hat{a}_0^\dagger + \sqrt{(G_1-1)(G_2-1)}\,\hat{a}_{v1},\\
\hat{a}_4 &= \sqrt{G_2}\,\hat{a}_{v3} + \sqrt{G_1(G_2-1)}\,\hat{a}_{v1}^\dagger\\
&\quad + \sqrt{(G_1-1)(G_2-1)}\,\hat{a}_0,
\end{aligned} \tag{11}$$

where G_1, G_2 are the power gains of cell$_1$, cell$_2$ (cell$_3$) respectively. Here we assume that the two FWM processes in the cell$_2$ and cell$_3$ have the same power gains for simplicity. The optical intensities ($N_i = \hat{a}_i^\dagger \hat{a}_i$ ($i = 1, 2, 3$ and 4)) for the individual beams $\hat{a}_1$, $\hat{a}_2$, $\hat{a}_3$ and $\hat{a}_4$ can be given by

$$\begin{aligned}
N_1 &= G_2(G_1-1)(N_0+1) + G_2\sqrt{G_1(G_1-1)}(\hat{a}_0\hat{a}_{v1} + \hat{a}_0^\dagger\hat{a}_{v1}^\dagger)\\
&\quad + \sqrt{G_2(G_1-1)(G_2-1)}(\hat{a}_0^\dagger\hat{a}_{v3} + \hat{a}_0\hat{a}_{v3}^\dagger),\\
N_2 &= G_1G_2N_0 + G_2\sqrt{G_1(G_1-1)}(\hat{a}_0\hat{a}_{v1} + \hat{a}_0^\dagger\hat{a}_{v1}^\dagger)\\
&\quad + \sqrt{G_1G_2(G_2-1)}(\hat{a}_0^\dagger\hat{a}_{v2}^\dagger + \hat{a}_0\hat{a}_{v2}),\\
N_3 &= G_1(G_2-1)(N_0+1)\\
&\quad + (G_2-1)\sqrt{G_1(G_1-1)}(\hat{a}_0\hat{a}_{v1} + \hat{a}_0^\dagger\hat{a}_{v1}^\dagger)\\
&\quad + \sqrt{G_1G_2(G_2-1)}(\hat{a}_0^\dagger\hat{a}_{v2}^\dagger + \hat{a}_0\hat{a}_{v2}),\\
N_4 &= (G_1-1)(G_2-1)N_0\\
&\quad + (G_2-1)\sqrt{G_1(G_1-1)}(\hat{a}_0\hat{a}_{v1} + \hat{a}_0^\dagger\hat{a}_{v1}^\dagger)\\
&\quad + \sqrt{G_2(G_1-1)(G_2-1)}(\hat{a}_0^\dagger\hat{a}_{v3} + \hat{a}_0\hat{a}_{v3}^\dagger),
\end{aligned} \tag{12}$$

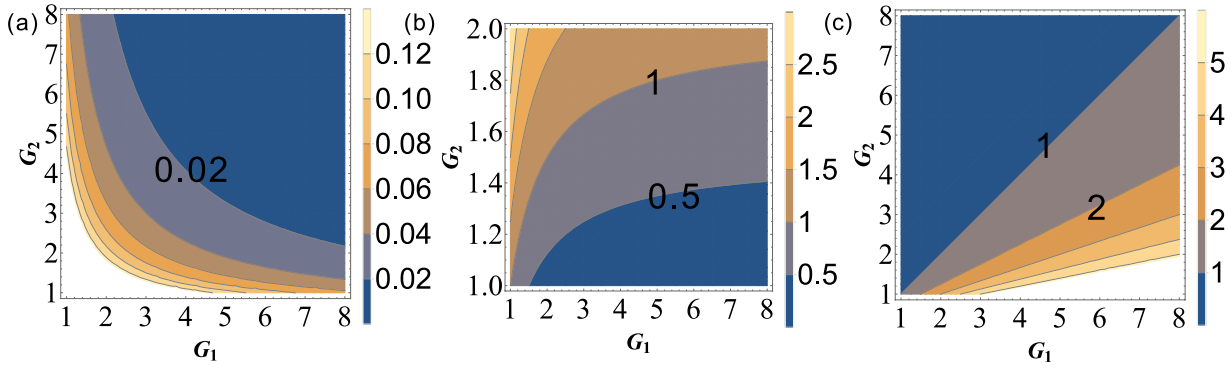

Figure 6. The contour plot (**a**) DS^3_{1234}; (**b**) DS^3_{12} and (**c**) DS^3_{14} and DS^3_{23}.

where $N_0 = \langle \hat{a}_0^\dagger \hat{a}_0 \rangle$. Here the second-order vacuum terms are omitted. It should be noted that the *DS* of the quadruple beams ($\hat{a}_1$, $\hat{a}_2$, $\hat{a}_3$ and $\hat{a}_4$) is given by

$$\begin{aligned} DS^3_{1234} &= \frac{Var(N_1 - N_4 - N_2 + N_3)_{FWM}}{Var(N_1 - N_4 - N_2 + N_3)_{SQL}} \\ &= \frac{1}{(2G_1 - 1)(2G_2 - 1)}, \end{aligned} \tag{13}$$

compared with Eq. (7), this cascaded scheme has also enhanced the quantum correlation of the system. The symmetrical dependence of the DS^3_{1234} on the gains is shown in Fig. 6(a) and it can be enhanced with the increasing of the gains G_1 and G_2, similar to the case of DS^2_{123}. The quantum correlation shared by the quadruple beams is present if $(2G_1 - 1)(2G_2 - 1) > 1$, i. e., $G_1 > 1$ or $G_2 > 1$. Next let us analyze all the possible PCs in this scheme and the triple correlations can also be obtained from the expressions of the PCs in the asymmetrical cascaded FWM scheme, for example, the DS for the triple beams ($\hat{a}_1$, $\hat{a}_2$ and $\hat{a}_4$) can be expressed as $DS^3_{134} = DS^2_{13} \frac{G_1 - 1 + G_1(G_2 - 1)}{(2G_3 - 1)(G_1 - 1) + G_1(G_2 - 1)}$. Therefore, we only focus on the PCs. PC between $\hat{a}_1$ and $\hat{a}_2$ can be quantified by

$$DS^3_{12} = \frac{2G_1G_2 - 2G_1 + 1}{2G_1 - 1}. \tag{14}$$

The region in which $DS^3_{12} < 1$ is shown in green denoted as (1, 2) in Fig. 5(b), the contour plot of the dependence of DS^3_{12} on the gains G_1 and G_2 is shown in Fig. 6(b). With the increasing of G_1, the value of G_2 on the boundary always increases and eventually saturates at the value of 2 (see the boundary given by $G_2 = 2 - 1/G_1$ in Fig. 5(b)). This is different from the asymmetrical scheme discussed above, where the value of G_2 on the boundary finally reaches 1. This is because here beams $\hat{a}_1$ and $\hat{a}_2$ from the first FWM process experience the same amount of amplification in the second and third FWM processes, which leads to their good noise balance, thus the performance of the PC with quantum correlation between beams $\hat{a}_1$ and $\hat{a}_2$ is not as sensitive to the G_2 as the one in the asymmetrical cascaded FWM scheme, where only beam $\hat{a}_2$ experiences the amplification, leading to noise unbalance. The study of DS^3_{12} presented above is actually the question of how to preserve the quantum correlation between beams $\hat{a}_1$ and $\hat{a}_2$ under the introduction of two FWMs which bring the deterioration effect to the quantum correlation by the quantum amplification of both the beams ($\hat{a}_1$, $\hat{a}_2$). The results shown in Figs 5(b) and 6(b) actually shows the boundary for the values of G_2 below which the quantum correlation can always be preserved as the value of G_1 increases. More interestingly, any value of G_2 more than 2 will eliminate the possibility of the existence of PC with quantum correlation between beams $\hat{a}_1$ and $\hat{a}_2$ regardless of the value of G_1.

PC between $\hat{a}_1$ and $\hat{a}_4$ ($\hat{a}_2$ and $\hat{a}_3$) can be quantified by

$$DS^3_{14} = \frac{2G_1 - 1}{2G_2 - 1}, \left(DS^3_{23} = \frac{2G_1 - 1}{2G_2 - 1} \right). \tag{15}$$

Eq. (15) is similar to the case of Eq. (10). The region in which $DS^3_{14} < 1$ ($DS^3_{23} < 1$) is shown in magenta denoted as ((1, 4), (2, 3)) in Fig. 5(b) and the contour plot is shown in Fig. 6(c). Therefore, beams $\hat{a}_1$ ($\hat{a}_2$) and $\hat{a}_4$ ($\hat{a}_3$) are quantum correlated within the magenta region ($G_1 < G_2$) in Fig. 5(b).

PC between $\hat{a}_1$ and $\hat{a}_3$ ($\hat{a}_2$ and $\hat{a}_4$) can be quantified by

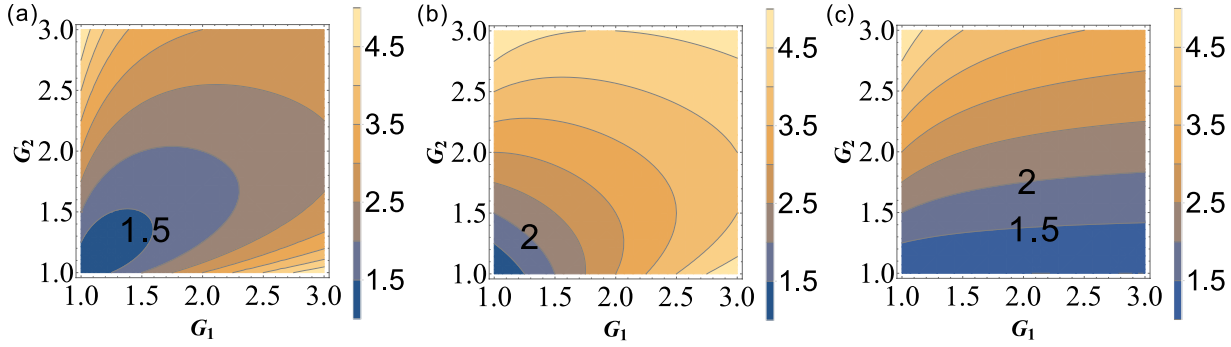

Figure 7. The contour plot of (**a**) DS^3_{13}; (**b**) DS^3_{24} and (**c**) DS^3_{34}.

$$\begin{aligned} DS^3_{13} &= \frac{-4G_1G_2 + 2G_1G_2^2 + 2G_1^2 - G_1 + G_2}{2G_1G_2 - G_1 - G_2}, \\ \left(DS^3_{24}\right. &= \left.\frac{2G_1G_2^2 + 2G_1^2 - 3G_1 - G_2 + 1}{2G_1G_2 - G_1 - G_2 + 1}\right). \end{aligned} \tag{16}$$

Eq. (16) is always larger than 1 for any value of G_1, $G_2 > 1$ as shown in the contour plot of DS^3_{13} and DS^3_{24} in Fig. 7(a) and (b). In this sense, there isn't any quantum correlation between beams $\hat{a}_1$ and $\hat{a}_3$ ($\hat{a}_2$ and $\hat{a}_4$) since DS^3_{13} (DS^3_{24}) is always larger than 1 for any value of G_1, $G_2 > 1$. The absence of $DS^3_{13} = 1$ ($DS^3_{24} = 1$) here compared with the red line in Fig. 1(b) is due to that both the beams $\hat{a}_1$ and $\hat{a}_3$ ($\hat{a}_2$ and $\hat{a}_4$) are amplified by the second and the third FWM processes independently.

PC between $\hat{a}_3$ and $\hat{a}_4$ can be quantified by

$$DS^3_{34} = \frac{2G_1G_2 - 1}{2G_1 - 1}. \tag{17}$$

The PC with quantum correlation between beams $\hat{a}_3$ and $\hat{a}_4$ will be absent because G_2 is always more than or equal to 1. This can be easily found if one looks at the functional form of Eq. (17). Its contour plot is shown in Fig. 7(c) in which the value of all the region is more than 1 for any G_1, $G_2 > 1$. As discussed above, for this symmetric cascaded scheme, there are three possible PCs with quantum correlation, namely DS^3_{12}, DS^3_{14} and DS^3_{23}. In addition, the existence of quantum correlation between beams $\hat{a}_1$ and $\hat{a}_2$ eliminates the possibility of the one between beams $\hat{a}_1$ ($\hat{a}_3$) and $\hat{a}_4$ ($\hat{a}_2$). In other words, beam $\hat{a}_1$ ($\hat{a}_2$) can't be simultaneously quantum correlated with beam $\hat{a}_2$ ($\hat{a}_1$) and $\hat{a}_4$ ($\hat{a}_3$). These effects in this symmetric scheme are similar to the above mentioned repulsion effect of quantum correlation between the PCs in the asymmetrical cascaded FWM process. Firstly, for the PC between beams $\hat{a}_1$ and $\hat{a}_2$, clearly, $cell_1$ will provide the correlation between them while $cell_2$ and $cell_3$ will destroy their quantum correlation by adding extra vacuum noise, thus $cell_1$, $cell_2$ ($cell_3$) can be viewed as the correlation mechanism provider and decorrelation mechanism provider respectively, thus the larger G_1 and smaller G_2 are preferred for the PC between beams $\hat{a}_1$ and $\hat{a}_2$. Secondly, for the case of the PC between $\hat{a}_1$ and $\hat{a}_4$ ($\hat{a}_2$ and $\hat{a}_3$), $cell_1$ will generate two thermal states which will destroy their quantum correlation by adding extra vacuum noise into the system while the $cell_3$ ($cell_2$) will make them quantum correlated through the FWM processes. In this case, $cell_1$, $cell_3$ ($cell_2$) can be viewed as the decorrelation mechanism provider and correlation mechanism provider respectively, thus the smaller G_1 and larger G_2 are preferred for the PC between beams $\hat{a}_1$ and $\hat{a}_4$ ($\hat{a}_2$ and $\hat{a}_3$). Finally, the complete opposite dependence of the PC between beams $\hat{a}_1$ and $\hat{a}_2$ and the PC between beams $\hat{a}_1$ and $\hat{a}_4$ ($\hat{a}_2$ and $\hat{a}_3$) on the gains results in the repulsion effect between the PCs of certain pairs. In the blank region of Fig. 5(b), all of the PCs have no quantum correlation since $DS^3_{12} \geq 1, DS^3_{13} \geq 1, DS^3_{14} \geq 1, DS^3_{23} \geq 1, DS^3_{24} \geq 1$ and $DS^3_{34} \geq 1$, however, the quantum correlation between the quadruple beams is still present.

Here we also give a summary of the theoretical predictions of Figs 5(b), 6 and 7. We plot the dependence of the (*A*) DS^3_{1234}; (*B*) DS^3_{12}; (*C*) DS^3_{13}; (*D*) DS^3_{14} and DS^3_{23}; (*E*) DS^3_{24} and (*F*) DS^3_{34} on the gain G_2 when $G_1 = 2.94$ ($cell_1$ gain in the experiment) in Fig. 8. DS^3_{1234} (trace *A*) can be enhanced with the increasing of G_2 which is consistent with Fig. 6(a), the value of DS^3_{12} (trace *B*) will be larger than 1 as long as $G_2 > 1.67$ which is consistent with the boundary ($G_2 = 2 - 1/G_1$) in Fig. 5(b), the value of DS^3_{14} and DS^3_{23} (trace *D*) will be smaller than 1 as long as $G_2 > 2.9$ which is consistent with Figs 5(b) and 6(c). In addition, DS^3_{13} (trace *C*), DS^3_{24} (trace *E*) and DS^3_{34} (trace *F*) are also consistent with Fig. 7(a–c) respectively.

We have also applied these theoretical predictions to the experimental results of the symmetrical cascaded scheme as shown in Fig. 9, the traces *A*, *B*, *C*, *D* and *E* are the measured DSs between $\hat{a}_3$ and $\hat{a}_4$, $\hat{a}_1$ and $\hat{a}_2$, $\hat{a}_1$ and $\hat{a}_4$, $\hat{a}_2$ and $\hat{a}_3$ and the quadruple beams respectively, the trace F is the corresponding normalized SQLs for traces $A \sim E$ (See the methods). The experimental results show $10\text{Log}(DS^3_{34}) = 5.9 \pm 0.3$ dB, $10\text{Log}(DS^3_{12}) = 3.8 \pm 0.6$ dB, $10\text{Log}(DS^3_{14}) = 0.1 \pm 0.4$ dB, $10\text{Log}(DS^3_{23}) = -0.2 \pm 0.7$ dB and $10\text{Log}(DS^3_{1234}) = -8.2 \pm 0.5$ dB at 0.6 MHz. For the

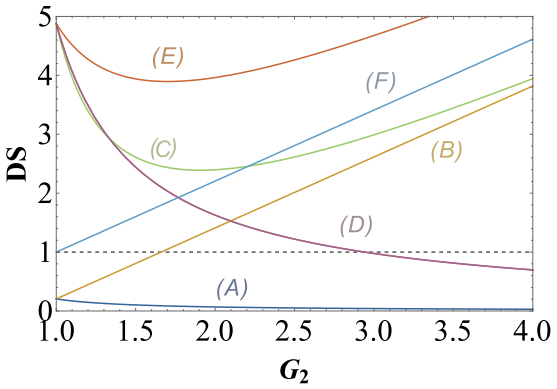

Figure 8. The dependence of (*A*) DS^3_{1234}; (*B*) DS^3_{12}; (*C*) DS^3_{13}; (*D*) DS^3_{14} and DS^3_{23}; (*E*) DS^3_{24} and (*F*) DS^3_{34} on the gain G_2 when $G_1 = 2.94$ ($cell_1$ gain in the experiment). The black dashed line: SQL.

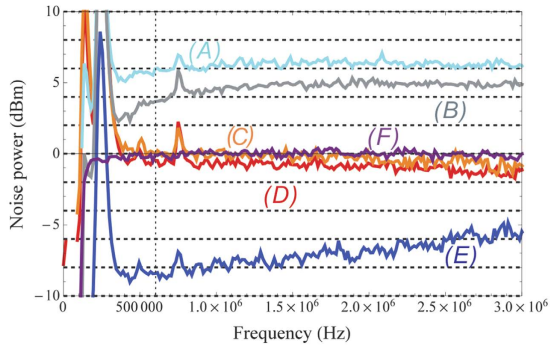

Figure 9. Experimentally measured (*A*) DS^3_{34}; (*B*) DS^3_{12}; (*C*) DS^3_{14}; (*D*) DS^3_{23}; (*E*) DS^3_{1234} and (*F*) the corresponding SQLs of the traces *A* ~ *E* in the symmetrical cascaded scheme. The vertical dashed line: 0.6 MHz.

experimental gains $G_1 \approx 2.94$ and $G_2 \approx 2.85$, the theoretical predictions give $10\text{Log}(DS^3_{34}) = 5.1$ dB, $10\text{Log}(DS^3_{12}) = 3.9$ dB, $10\text{Log}(DS^3_{14}) = 0.2$ dB, $10\text{Log}(DS^3_{23}) = 0.2$ dB and $10\text{Log}(DS^3_{1234}) = -13.6$ dB. As we can see, although these theoretical predictions do not perfectly agree with the experimental results at 0.6 MHz, they still give a rough estimation of the relationship between the obtained experimental noise power traces.

Discussion

The PCs existed in the asymmetrical cascaded scheme and symmetrical cascaded scheme are both studied. We found that the symmetrical cascaded scheme has the following distinctions compared with the asymmetrical cascaded scheme: (1) Quantum enhancement. The DS of the quadruple beams in the symmetrical cascaded scheme (Eq. 13) has quantum enhancement compared with the one of the triple beams in the asymmetrical cascaded scheme (Eq. 7) with the same gains; (2) Boundary effect. The boundary of the PC with quantum correlation between beams $\hat{a}_1$ and $\hat{a}_2$ in the asymmetrical cascaded FWM scheme shown in Fig. 1(b) is obviously different from the one of the symmetrical cascaded FWM scheme shown in Fig. 5(b). This is because here beams $\hat{a}_1$ and $\hat{a}_2$ from the first FWM process experience the same amount of amplification in the second and third FWM processes, which leads to their good noise balance, thus the performance of the PC with quantum correlation between beams $\hat{a}_1$ and $\hat{a}_2$ is not as sensitive to the G_2 as the one in the asymmetrical cascaded FWM scheme, where only beam $\hat{a}_2$ experiences the amplification, leading to noise unbalance. (3) SQL Approaching. The PC between beams $\hat{a}_1$ and $\hat{a}_3$ in the asymmetrical cascaded FWM scheme is clearly different from the one in the symmetrical cascaded FWM scheme. The PC between beams $\hat{a}_1$ and $\hat{a}_3$ in the asymmetrical cascaded FWM scheme can approach its corresponding SQL (see the trace *C* in Fig. 3), while the PC between beams $\hat{a}_1$ and $\hat{a}_3$ in the symmetrical cascaded FWM scheme is always much higher than its corresponding SQL (see the trace *C* in Fig. 8). This is because in the asymmetrical cascaded FWM scheme only one beam $\hat{a}_3$ is amplified by the second FWM process, while in the symmetrical cascaded FWM scheme both of the beams $\hat{a}_1$ and $\hat{a}_3$ are amplified by the second and third FWM processes independently.

In summary, we have theoretically characterized the performance of the PCs from the multiple quantum correlated beams and analyzed the dependence of all the PCs on the system intensity gains based on two different cascaded FWM processes. For both cases, we have theoretically predicted the so called repulsion effect of

quantum correlation between the PCs of the cascaded systems. Our results presented here can be applied to the classification and application of the quantum states generated from the cascaded FWM processes.

Methods

Experimental measurements of PCs. The output beams $\hat{a}_i$ ($i = 1, 2, 3,$ and 4) from the cascaded FWM processes are sent to the photodetectors and their noise power values N_i ($i = 1, 2, 3,$ and 4) are measured. One beam is subtracted from the other beam in the pairwise beams and thus the intensity-difference squeezing shared by the pairwise beams is measured. In addition, the SQL of the measured pairwise beams can be measured in this way by using a beam in a coherent state with a power equal to the total power of the measured pairwise beams impinging on the photodetectors. We then split it with a 50/50 beamsplitter, direct the obtained beams into two photodetectors. and record the noise power of the differential photocurrent. This balanced detection system makes it possible to cancel all the sources of classical noise and obtain a measure of the SQL.

References

1. Greenberger, D. M., Horne, M. A. & Zeilinger, A. Multiparticle Interferometry and the Superposition Principle. *Phys. Today* **46(8),** 22–29 (1993).
2. Braunstein, S. L. & Loock, P. V. Quantum information with continuous variables. *Rev. Mod. Phys.* **77,** 513–517 (2005).
3. Coffman, V., Kundu, J. & Wootters, W. K. Distributed entanglement. *Phys. Rev. A* **61,** 052306 (2000).
4. Amico, L., Fazio, R., Osterloh, A. & Vedral, V. Entanglement in many-body systems. *Rev. Mod. Phys.* **80,** 517–576 (2008).
5. Borsten, L., Dahanayake, D., Duff, M. J., Rubens, W. & Ebrahim, H. Freudenthal triple classification of three-qubit entanglement. *Phys. Rev. A* **80,** 032326 (2008).
6. Acn, A., Bruß, D., Lewenstein, A. & Sanpera, A. Classification of Mixed Three-Qubit States. *Phys. Rev. Lett.* **87,** 040401 (2001).
7. Borsten, L., Dahanayake, D., Duff, M. J., Marrani, A. & Rubens, W. Four-Qubit Entanglement Classification from String Theory. *Phys. Rev. Lett.* **105,** 100507 (2010).
8. Rigolin, G., de Oliveira, T. R. & de Oliveira, M. C. Operational classification and quantification of multipartite entangled states. *Phys. Rev. A* **74,** 022314 (2006).
9. McCormcik, C. F., Boyer, V., Arimondo, E. & Lett, P. D. Strong relative intensity squeezing by four-wave mixing in rubidium vapor. *Opt. Lett.* **32,** 178–180 (2007).
10. Boyer, V., Marino, A. M., Pooser, R. C. & Lett, P. D. Entangled Images from Four-Wave Mixing. *Science* **321,** 544–547 (2008).
11. Embrey, C. S., Turnbull, M. T., Petrov, P. G. & Boyer, V. Observation of Localized Multi-Spatial-Mode Quadrature Squeezing. *Phys. Rev. X* **5,** 031004 (2015).
12. Lawrie, B. J., Evans, P. G. & Pooser, R. C. Extraordinary Optical Transmission of Multimode Quantum Correlations via Localized Surface Plasmons. *Phys. Rev. Lett.* **110,** 156802 (2013).
13. Pooser, R. C. & Lawrie, B. Ultrasensitive measurement of microcantilever displacement below the shot-noise limit. *Optica* **2,** 393–399 (2015).
14. Marino, A. M., Boyer, V., Pooser, R. C., Lett, P. D., Lemons, K. & Jones, K. M. Delocalized Correlations in Twin Light Beams with Orbital Angular Momentum. *Phys. Rev. Lett.* **101,** 093602 (2008).
15. Vogl, U., Glasser, R. T. & Lett, P. D. Advanced detection of information in optical pulses with negative group velocity. *Phys. Rev. A* **86,** 031806(R) (2012).
16. Vogl, U., Glasser, R. T., Glorieux, Q., Clark, J. B., Corzo, N. V. & Lett, P. D. Experimental characterization of Gaussian quantum discord generated by four-wave mixing. *Phys. Rev. A* **87,** 010101(R) (2013).
17. Glasser, R. T., Vogl, U. & Lett, P. D. Stimulated Generation of Superluminal Light Pulses via Four-Wave Mixing. *Phys. Rev. Lett.* **108,** 173902 (2012).
18. Corzo, N. V., Marino, A. M., Jones, K. M. & Lett, P. D. Noiseless Optical Amplifier Operating on Hundreds of Spatial Modes. *Phys. Rev. Lett.* **109,** 043602 (2012).
19. Marino, A. M., Pooser, R. C., Boyer, V. & Lett, P. D. Tunable delay of Einstein-Podolsky-Rosen entanglement. *Nature* **457,** 859–862 (2009).
20. Pooser, R. C., Marino, A. M., Boyer, V., Jones, K. M. & Lett, P. D. Low-Noise Amplification of a Continuous-Variable Quantum State. *Phys. Rev. Lett.* **103,** 010501 (2009).
21. Jing, J., Liu, C., Zhou, Z., Ou, Z. Y. & Zhang, W. Realization of a nonlinear interferometer with parametric amplifiers. *Appl. Phys. Lett.* **99,** 011110 (2011).
22. Hudelist, F., Kong, J., Liu, C., Jing, J., Ou, Z. & Zhang, W. Quantum metrology with parametric amplifier-based photon correlation interferometers. *Nature Comm.* **5,** 3049 (2014).
23. Clark, J. B., Glasser, R. T., Glorieux, Q., Vogl, U., Li, T., Jones, K. M. & Lett, P. D. Quantum mutual information of an entangled state propagating through a fast-light medium. *Nature Photon.* **8,** 515–519 (2014).
24. Vogl, U., Glasser, R. T., Clark, J. B., Glorieux, Q., Li, T., Corzo, N. V. & Lett, P. D. Advanced quantum noise correlations. *New J. Phys.* **16,** 013011 (2014).
25. Qin, Z., Cao, L., Wang, H., Marino, A. M., Zhang, W. & Jing, J. Eperimental Generation of Multiple Quantum Correlated Beams from Hot Rubidium Vapor. *Phys. Rev. Lett.* **113,** 023602 (2014).
26. Jasperse, M., Turner, L. D. & Scholten, R. E. Relative intensity squeezing by four-wave mixing with loss: an analytic model and experimental diagnostic. *Opt. Express* **19,** 3765–3774 (2011).
27. Marino, A. M., Boyer, V., McCormick, C. F. & Lett, P. D. Effect of Probe-Conjugate Delay on the Spectrum of Squeezed Light, doi: 10.1364/CQO.2007.CSuA25.

Acknowledgements

This work was supported by the National Natural Science Foundation of China under Grant Nos. 91436211, 11374104 and 10974057, the SRFDP (20130076110011), the Program for Professor of Special Appointment (Eastern Scholar) at Shanghai Institutions of Higher Learning, the Program for New Century Excellent Talents in University (NCET-10-0383), the Shu Guang project supported by Shanghai Municipal Education Commission and Shanghai Education Development Foundation (11SG26), the Shanghai Pujiang Program under Grant No. 09PJ1404400, the Scientific Research Foundation of the Returned Overseas Chinese Scholars, State Education Ministry, National Basic Research Program of China (Grant No. 2016YFA030213), and Program of State Key Laboratory of Advanced Optical Communication Systems and Networks (2016GZKF0JT003).

Author Contributions

J.J. conceived the idea. H.W., L.C. and J.J. performed the analytical calculations and the experimental measurements. J.J. and H.W. co-wrote the manuscript. All authors reviewed the manuscript.

Additional Information

Competing financial interests: The authors declare no competing financial interests.

How to cite this article: Wang, H. *et al.* Characterization of Pairwise Correlations from Multiple Quantum Correlated Beams Generated from Cascaded Four-Wave Mixing Processes. *Sci. Rep.* **7**, 40410; doi: 10.1038/srep40410 (2017).

Publisher's note: Springer Nature remains neutral with regard to jurisdictional claims in published maps and institutional affiliations.